Soft Matter

Dilute solution structure of bottlebrush polymers

Journal:	*Soft Matter*
Manuscript ID	SM-ART-01-2019-000033.R1
Article Type:	Paper
Date Submitted by the Author:	22-Jan-2019
Complete List of Authors:	Dutta, Sarit; University of Illinois at Urbana-Champaign, Chemical and Biomolecular Engineering Wade, Matthew; University of Illinois at Urbana-Champaign, Chemical and Biomolecular Engineering Walsh, Dylan; University of Illinois at Urbana-Champaign, Department of Chemical and Biomolecular Engineering Guironnet, Damien; University of Illinois at Urbana-Champaign, Department of Chemical and Biomolecular Engineering Rogers, Simon; University of Illinois at Urbana-Champaign, Chemical and Biomolecular Engineering Sing, Charles; University of Illinois at Urbana-Champaign, Department of Chemical and Biomolecular Engineering

Journal Name

ARTICLE TYPE

Cite this: DOI: 10.1039/xxxxxxxxxx

Dilute solution structure of bottlebrush polymers†

Sarit Dutta, Matthew A. Wade, Dylan J. Walsh, Damien Guironnet, Simon A. Rogers, and Charles E. Sing*

Received Date
Accepted Date

DOI: 10.1039/xxxxxxxxxx

www.rsc.org/journalname

Bottlebrush polymers are a class of macromolecules that has recently found use in a wide variety of materials, ranging from lubricating brushes and nanostructured coatings to elastomeric gels that exhibit structural color. These polymers are characterized by dense branches extending from a central backbone, and thus have properties distinct from linear polymers. It remains a challenge to specifically understand conformational properties of these molecules, due to the wide range of architectural parameters that can be present in a system, and thus there is a need to accurately characterize and model these molecules. In this paper, we use a combination of viscometry, light scattering, and computer simulations to gain insight into the conformational properties of dilute bottlebrush polymers. We focus on a series of model bottlebrushes consisting of a poly(norbornene) (PNB) backbone with poly(lactic acid) (PLA) side chains. We demonstrate that intrinsic viscosity and hydrodynamic radius are experimental observations *sensitive* to molecular architecture, exhibiting distinct differences with different choices of branch and backbone lengths. Informed by the atomistic structure of this PNB-PLA system, we rationalize a coarse-grained simulation model that we evaluate using a combination of Brownian Dynamics and Monte Carlo simulations. We show that this exhibits quantitative matching to experimental results, enabling us to characterize the overall shape of the bottlebrush via a number of metrics that can be extended to more general bottlebrush architectures.

1 Introduction

Bottlebrush polymers are a class of highly branched macromolecules consisting of a main backbone chain with a high density of polymer side chains (see Fig. 1). The densely-branched architecture of bottlebrush polymers imparts molecular, and consequently material, properties that are distinct from typical linear polymers; the grafted side chains enhance the stiffness of the overall chain and force the backbone to adopt an extended conformation. In the case of bottlebrush melts, this leads to a suppression of molecular entanglements [1–3] and significantly lowers the conformational degrees of freedom of these large polymers compared to linear polymer of similar length.

A wide range of functional materials have leveraged these unique properties in a wide range of applications; for example, the decreased conformational degrees of freedom has been used in the context of surface-adsorbed bottlebrush materials, such as molecular pressure sensors that detect film pressure at liquid solid interfaces, [4,5] pressure sensitive adhesives, [6] pH-responsive surfaces, [7] and stimuli-responsive molecular brushes. [8] The suppression of molecular entanglements has been used to great effect in bottlebrushes with block copolymer constituents, which undergo microphase separation to form well-ordered domains. [9–11] The reduced entanglement and stretched conformation allows these domains to reach length scales appropriate for photonic [12–14] and phononic crystals, [15] that would otherwise be kinetically difficult to form with linear block copolymers. This reduced entanglement effect is also exploited in designing low modulus elastomers capable of strain-hardening and sustaining large deformation, with applications in artificial muscle development and camouflage technology via strain-adaptive structural coloration. [16–20]

Bottlebrush architectures are also encountered in biological systems, often in environments where they play a functional role of providing structural support and altering mechanical properties. For example, *aggrecan*, a proteoglycan with a bottlebrush-like structure occurring in cartilage, is partly responsible for controlling the mechanical strength of cartilage via its interaction with collagen fibres. [21] Similarly, *neurofilaments* provide structural support to myelinated axons in vertebrate nerve cells via hydrogelation of the strongly interacting side chains. [22]

Due to the utility of bottlebrush polymers, it is crucial to understand how to design their architecture and chemistry to yield desired material properties. This represents a challenge to both

* *Department of Chemical and Biomolecular Engineering, University of Illinois at Urbana-Champaign, Urbana, Illinois 61801, USA. E-mail: cesing@illinois.edu*

† Electronic Supplementary Information (ESI) available: [details of any supplementary information available should be included here]. See DOI: 10.1039/b000000x/

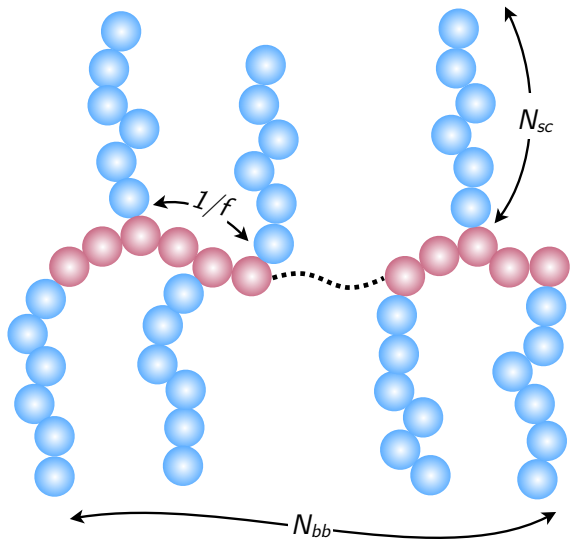

Fig. 1 Schematic of a bottlebrush model showing the architectural parameters. Note that in our study $f = 1$, i.e. each backbone monomer carries a side chain.

polymer chemists and polymer physicists, which has received a significant amount of interest over the past few decades.[2,23–37]

For polymer synthesis, the primary challenge has been to increase the versatility of the bottlebrush chemistry while also developing well-controlled polymerization schemes to obtain bottlebrushes with monomodal molecular weight distributions.[10,11,38] For most chemistries, this limits the backbone degree of polymerization (DP) to ca. 1000 monomers with a side-chain DP of 100–200, however individual examples of longer backbones have been reported.[39]

For polymer physicists, the overall challenge is the sheer number of choices for tuning the macromolecular architecture and chemistries, which represents a large parameter space that makes Edisonian molecular design inefficient. For example, it is possible to have varying graft densities[40] and backbone topologies[41]; constituent chains can be of varying flexibility[42,43] or incorporate block copolymers that exhibit intramolecular phase separation.[3,44,45] Similarly, bottlebrushes with dendritic side chains[46] and gradients in side chain DP[47,48] have also been considered.

The preceding discussion illustrates the need to have theoretical or computational approaches to complement synthetic efforts, so that properties can be predicted and designed without the need for extensive synthesis. However, even the conformational attributes of an individual bottlebrush chain in dilute solution remain unsettled in the literature. The main goal has been to understand molecular conformations using information associated with the molecular architecture (the grafting density f, the length of the backbone N_{bb}, and the length of the side chains N_{sc}) to obtain conformational measures (radius of gyration, R_G, hydrodynamic radius, R_H, intrinsic viscosity, $[\eta]$, persistence length, ℓ_p and bottlebrush diameter, D).

Theoretical efforts have focused on scaling approaches, which extend classical random-walk and "blob" arguments to bottlebrush architectures. Birshtein, et al.[23] initially predicted straightforward $R \sim N_{bb}^{3/5}$ scaling in both θ and good solvents, based on a "superblob" argument that arose from the prediction that $\ell_p/D \sim \mathcal{O}(1)$. Indeed, the dependence of R on N_{sc}, f, and solvent quality was predicted to be weak. This shows some inconsistency with later simulation and theoretical work,[49–55] however Monte Carlo simulations have placed the backbone size exponent to be in the range of 0.6 – 0.7.[52,54,56–58] Alternative scaling arguments by Fredrickson[24], who considered the related case of surfactant-associated polymer chains, predicted the effects of progressively increasing the grafting density f as moving through three regimes; a low grafting density where the bottlebrush appears coil-like ($f \ll N_{sc}^{-9/10}$), an intermediate grafting density ($N_{sc}^{-9/10} \ll f \ll N_{sc}^{-3/5}$) where the conformation is still coil-like yet expanded locally due to the side-chain interactions, and a high grafting density ($f \gg N_{sc}^{-3/5}$) where the bottlebrush becomes wormlike (semiflexible), characterized by a persistence length $\ell_p \sim f^{17/8} N_{sc}^{15/8}$.[24] Some agreement with molecular dynamics simulations have been observed.[59] Alternative approaches have also been used to understand bottlebrush structure, including perturbative methods,[60] self-consistent field theory,[61] and renormalization group methods.[62,63] Indeed, while most recent work has focused on models for dense melts,[64–71] there remains a need for further insight into dilute-solution bottlebrush structure.

The connection between these predictions and experimental systems remains sparse in the literature, but qualitative trends from both experiments and computer simulations suggest that the overall size and persistence length of bottlebrushes does increase due to the presence of side chains.[7,35,72–74] In particular, both SANS[75] and light scattering and viscosity[76] have shown evidence that ℓ_p can increase by an order of magnitude as the length of side chains increases. In case of molecules with dendronized side chains (upto third generation), light scattering studies[77,78] have shown a modest increase in ℓ_p; the overall conformation appearing more like a semiflexible chain rather than a rigid rod. There are challenges associated with extracting a "true" persistence length that does not change with the overall length of the chain, as evidenced by extensive molecular simulations.[79–83] However, the *wormlike cylinder model* appears to work quite well in extracting a persistence length from experimental data, and indeed show a pronounced effect of side-chains.[76,84] Nevertheless, there are experimental results that show instead that the ℓ_p remains essentially unchanged despite significant increase in N_{sc}.[31]

The large volume of experimental and theoretical work remains rife with conflicting observations.[23,24,30–32,35,49–54,59,61,74,75,85] Many of these issues have been discussed at length in a recent review by Binder et al.[86] This is in part due to the idealization required to make progress with theory, which is compounded by the reliance on experimental characterization that does not directly image the bottlebrush chains but instead infers structure from model predictions. Furthermore, efforts to include simulation data have often used similarly-idealized molecular models, that rarely invoke the specific chemistry used in a given bottlebrush in favor of universal statements.

In this work, we show that a combined approach of chem-

istry, characterization, and simulation can provide insight into the structure of bottlebrushes over a wide range of molecular parameters. We consider the specific chemistry of poly(norbornene) (PNB) backbones with poly(lactic acid) (PLA) side chains, so that we can exercise *precise* synthetic control over backbone and side-chain lengths. We subsequently focus on intrinsic viscosity, which we show to be *highly sensitive* to these architectural changes, providing a set of experimental data that both informs and validates the results of molecular simulation. In addition, experimental measurements of hydrodynamic radius from dynamic light scattering are presented as well. These are ultimately compared to Brownian Dynamics simulations that are explicitly parameterized based on known quantities for PNB and PLA (i.e. molecular structure, ℓ_p), and exhibit quantitative matching to experimental data that reflects the synthesized molecular architecture. Significantly, we are able to match computer simulations and experimental intrinsic viscosity measurements spanning a broad range of *experimentally-relevant* bottlebrush architectures, with a simulation model parameterized directly from the bottlebrush chemistry. This contrasts with prior efforts, which have focused on asymptotic limits or scaling laws that provide physical intuition; these are unable to quantitatively predict and visualize the conformations of synthesized bottlebrushes, which are not typically long enough to exhibit universal behavior. We show that a combined experimental/computational approach is able to provide predictions for the molecular structure of bottlebrushes in the synthetically-accessible window of molecular architectures, which can be used to calculate size and shape parameters that are crucial to molecular engineering applications yet difficult to predict from prior theoretical or experimental approaches.

2 Methods

2.1 Materials and instrumentation

Reactions were performed in an argon-filled glovebox (O_2 < 2 ppm, H_2O < 0.5 ppm) at room temperature using oven dried glassware. *rac*-Lactide (Aldrich) was used as received. THF was dried using a commercial solvent purification system. 1,8-diazabicyclo[5.4.0]undec-7-ene (DBU) (Aldrich) was distilled prior to use. [(H_2IMes)(3-Br-py)$_2$(Cl)$_2$Ru=CHPh], G3 was synthesized according to literature.[87] 5-Norbornene-2-methanol and 5-norbornene-2-(methylbenzoate) were synthesized according to literature (mixture of 20% exo/endo used).[36,88] Gel Permeation Chromatography (GPC) was performed using a Tosoh Ecosec HLC-8320GPC at 40 °C fitted with a reference column (6.0 mm ID × 15 cm), a guard column (6.0 mm ID × 4.0 cm × 5 μm), and two analytical columns (7.8 mm ID × 30 cm × 5 μm). The reference flow rate is 0.5 ml/min while the analytical column is at 1.0 ml/min. THF (HPLC grade) was used as the eluent, and polystyrene standards (15 points ranging from 500 Da to 8.42 $\times 10^6$ Da) were used as the general calibration. An additional calibration was created for specifically for linear polylactic acid and only used for linear polylactic acid (10 points ranging from 500 Da to 10^4 Da).

2.2 Synthesis

A representative procedure for bottlebrush synthesis (based on Ref. 48): To an oven-dried round bottom flask, lactide (12.86 g, 96 mmol) and 5-norbornene-2-methanol (158 mg, 1.27 mmol) dissolved in 96 mL of THF. Polymerization was initiated by adding DBU (64.4 mg, 0.42 mmol) dissolved in 1 mL of THF. This reaction mix till the desired arm length was reached (60 min for PLA DP = 70) at which time $B(OH)_3$ (523 mg, 8.46 mmol) in 36.5 mL of THF was added to the reaction mixture. An aliquot was removed for GPC analysis. At this point the large scale ROP was divided into 8 smaller ROMP reactions in which different amounts of G3 were added, i.e. different backbone lengths (backbone sweep). For example: ROMP was initiated by adding G3 (14.03 mg, 0.02 μmol for $n_{bb} = 10$) in 0.5 mL of THF. After 30 min, a large excess of ethyl vinyl ether (large excess with respect to [Ru]) was added to the reaction mixture. The reaction mixture was then poured into cold methanol (−30 °C) and a centrifuge was used to isolate the resulting polymer. The polymer was dried under vacuum and then analyzed by GPC. In order to get $B(OH)_3$ to dissolve into THF, the solution was heated to ∼ 80 – 90°C (BP of THF is 66 °C, use a sealed vial that can handle pressure buildup) till all the $B(OH)_3$ dissolved and allowed to cool back to room temperature before use. Avoid rapid cooling of the solution, as it will cause $B(OH)_3$ to drop out of solution.

A representative procedure for ROMP of 5-norbornene-2-(methylbenzoate) (based on Ref. 89): In an argon filled glovebox, 5-norbornene-2-(methylbenzoate) (300 mg, 1.31 mmol) was dissolved into 38 mL of anhydrous THF. A separate stock solution of G3 was generated such that 2 mL of solution provide the amount of G3 needed for a specific degree of polymerization (DP) (ex. $N = 200$, 5.81 mg G3/2 mL of THF). The G3 solution 2 mL was added to the 5-norbornene-2-(methylbenzoate) solution to initiate the polymerization. The mixture was stirred vigorously after 5 min, a large excess of ethyl vinyl ether was added to the reaction mixture. The reaction mixture was then poured into methanol and a centrifuge was used to isolate the resulting polymer ($N < 72$ were purified by column chromatography as they did not precipitate). The polymer was dried under vacuum and then analyzed by GPC.

2.3 Bottlebrush Characterization

Dilute solutions were prepared by dissolving bottlebrushes in filtered chlorobenzene to form bulk solutions with concentrations ranging from 12 mg/mL to 15 mg/mL. The solutions were mixed on a shaker table for approximately 12 h at 200 rpm to ensure even dispersal of bottlebrushes. Chlorobenzene (CB) was chosen as the solvent for two reasons — (i) PLA bottlebrushes could be readily dissolved in CB, and (ii) CB has a relatively high boiling point compared to other organic solvents, which reduces the effects of solvent evaporation.

The viscosity of each solution was measured at 30 °C using one of two Cannon-Fenske capillary viscometers with different conversion constants. The viscometers were suspended in a heated ethylene glycol bath to prevent temperature variation. The viscosity was measured for bottlebrush solutions with concentrations

between 2 mg/mL and 15 mg/mL. Change in concentration was achieved by removing bottlebrush solution from the viscometer and adding solvent to the viscometer. The intrinsic viscosity $[\eta]$ was determined by fitting these concentration sweeps to Kraemer[90] and Huggins[91] models.

Dynamic light scattering was performed using a Malvern Zetasizer Nano S90 to determine center-of-mass diffusion coefficient and hydrodynamic radius of bottlebrush molecules. The setup consisted of a 4 mW HeNe laser with a wavelength of 633 nm and an Avalanche photodiode located at a fixed scattering angle of 90° relative to the incident laser beam.[92–94] We note that performing scattering at this relatively large wave-vector may introduce some wave-vector dependence on the hydrodynamic radius; however, our results indicate that these measurements are consistent with intrinsic viscosity and computer simulations and thus we do not pursue studying this wave-vector dependence. Bottlebrush samples were diluted in chlorobenzene to concentrations ranging from 4 mg/mL to 12 mg/mL and loaded into glass cuvettes. Prior to testing, the samples were heated to a temperature of 30 °C at which point they were allowed to reach thermal equilibrium over a period of 5 min. During each test, the intensity of light as a function of time was recorded and compared with itself to generate an autocorrelation function. Using the Zetasizer software package provided by Malvern, a set of exponential decay functions were fit to the autocorrelation function according to the cumulants method. From the center-of-mass diffusivity was determined from the exponential decay coefficient, which was in turn used to calculate the hydrodynamic radius according to the Stokes-Einstein equation. A more detailed description of this process is provided as ESI†.

2.4 Simulation Protocol

Computer simulations were performed on a coarse-grained bead-spring representation of bottlebrush polymers, parameterized to the specific polymers used. Here we outline the general simulation model, and discuss the parameterization in Section 2.5. A detailed description of the simulation method is provided as ESI†.

A schematic of our computational model is shown in Fig. 1. The backbone consists of N_{bb} beads; each backbone bead carries one side chain consisting of N_{sc} beads. These beads experience a potential $U = U_s + U_{ev} + U_b$ that describes the intramolecular interactions present in the system; bead connectivity U_s, bead excluded volume U_{ev}, and a bending potential U_b. The connectivities between the beads were implemented via finitely extensible nonlinear elastic (FENE) spring forces derived from the potential

$$U_s = -\frac{1}{2}k_s r_{\max}^2 \log\left[1-\left(\frac{r_{ij}}{r_{\max}}\right)^2\right], \quad r_{ij} < r_{\max}. \qquad (1)$$

Here, the spring constant is $k_s = 30\varepsilon/\sigma^2$ and the maximum spring extension is $r_{\max} = 1.5\sigma$, where r_{ij} is the distance between two connecting beads and σ and ε are the length and energy parameters, respectively.[95]

Excluded volume interaction among the beads was represented using the Weeks-Chandler-Anderson[96] potential for simulations in a very good (athermal) solvent. The Lennard-Jones potential truncated at 2.5σ was used for simulations under non-athermal conditions. A bending potential of the standard cosine form[97] was applied only to the backbone beads, with a bending constant $k_b = 0.5k_BT$, where k_B is the Boltzmann constant and T is the absolute temperature. Although a bending potential for the backbone beads is not necessary for a generic bottlebrush model, we included it to account for the specific polymer chemistries considered in the experimental system.

We used standard Brownian Dynamics[98] (BD) augmented with global Monte Carlo (MC) moves to evolve the bead positions. For computational expediency we neglected hydrodynamic interaction (HI) between the beads in the BD step. Two kinds of MC moves, (i) backbone *pivot* and (ii) side chain *double bridging* were used periodically after several BD steps to induce rapid global conformational changes. This is similar in spirit to what Auhl et al[97] advocated for equilibrating configurations in polymer melts, except that we chose to retain the MC moves for the production run as well. The time step for advancing the beads during a single BD step was 10^{-4}, with a total duration of 10^8 time steps or more.

Neglecting HI during BD as well as the use of MC moves costs us by losing the fidelity of temporal evolution, albeit in a way that still maintains the equilibrium set of configurations. We justify this approximation by noting that our simulations were used solely to obtain an equilibrium distribution of bottlebrush conformations, with which we calculated equilibrium quantities. Static properties such as bottlebrush extension and radius of gyration were calculated based on equilibrium averages not affected by ignoring HI, and dynamic properties such as hydrodynamic radius R_h and intrinsic viscosity $[\eta]$ reinject hydrodynamics in the context of Kirkwood theory, which can be evaluated based solely on equilibrium configurations.

Center-of-mass diffusivity was calculated based on the equilibrium conformations using the Kirkwood formula,[99] from which R_h was evaluated using the Stokes-Einstein relation. Such a calculation yields an upper-bound estimate[100] for D and thus a lower-bound estimate for R_h. A similar calculation can be performed for $[\eta]$, which was calculated using an expression derived by Tsuda[101,102] based on a non-preaveraged version of Kirkwood theory. We also included a correction factor to Tsuda's expression provided by de la Torre and coworkers.[103] Calculations of R_h and $[\eta]$ are performed over the entire ensemble of equilibrium conformations in simulation, and thus capture the full range of conformational fluctuations. These are not exact expressions, with approximations and corrections discussed in the literature.[99,100,104] Nevertheless, we performed checks on the determination of R_h and $[\eta]$ by simulating linear polymers to determine that mass scaling exponents reproduce the standard Zimm predictions.[105] The relevant expressions for determining R_h and $[\eta]$ from equilibrium conformations as well as plots showing verification of mass scaling exponents based on these expressions are provided as ESI†.

2.5 Bottlebrush Parameterization

Our combined approach of chemistry, characterization, and simulation is built on careful parameterization of the specific chemistries used for the bottlebrush synthesis in the context of the

Definition	Experiment	Simulation
Backbone degree of polymerization	n_{bb}	$1.1(N_{bb}-1)^*$
Side chain degree of polymerization	n_{sc}	$2.17(N_{sc}-1)^*$
Backbone molecular weight	$M_{bb}{}^\ddagger$	$134.6(N_{bb}-1)$
Side chain molecular weight	$M_{sc}{}^\ddagger$	$161.8(N_{sc}-1)$
Total molecular weight	$M^\ddagger$	$134.6(N_{bb}-1)+161.8N_{sc}N_{bb}$
Simulation length scale	0.67 nm	σ

* rounded off to nearest integer
‡ in Dalton

Table 1 Mapping between simulation and experimental parameters.

idealized bead-spring simulation model. Our parameterization procedure is built on mapping the simulation variables to their corresponding experimental counterparts, so that we can directly simulate a bottlebrush polymer of known molecular weight and backbone/side chain DP. This mapping is not necessarily unique, but we demonstrate that it yields reasonable quantitative matching between simulation and experiment. This correspondence enables us to directly visualize molecular bottlebrush conformations consistent with the bulk experimental observables.

In our model, N_{bb} backbone beads represent n_{bb} chemical repeat units of PNB, such that the molecular weight of the backbone is M_{bb}. We similarly consider side chains N_{sc} beads long to represent n_{sc} chemical repeat units of PLA, such that the molecular weight per side chain is M_{sc}. The entire simulated bottlebrush is thus represented by $N = N_{bb}(1+N_{sc})$ beads for a total molecular weight of $M = M_{bb}+n_{bb}M_{sc}$.

The Kuhn length, b_K, of a linear polymer can be obtained from its characteristic ratio, C_∞, the length of its constituent bonds, l_b, and the bond angle (complementary), θ, using the relation[105] $b_K/l_b = C_\infty/\cos(\theta/2)$. For PLA, $C_\infty = 6.5$[106], and assuming $\theta \approx 68^\circ$, we have $b_{K,\mathrm{PLA}}/l_{b,\mathrm{PLA}} = 7.84$, i.e. there are ca. 7.84 chemical bonds per Kuhn segment of PLA. Further assuming $l_{b,\mathrm{PLA}} \approx 0.154$ nm, we obtain $b_{K,\mathrm{PLA}} = 7.84 \times l_{b,\mathrm{PLA}} = 1.2$ nm. An analogous calculation for PNB with $C_\infty = 12.1$[107] and $\theta \approx 68^\circ$ shows $b_{K,\mathrm{PNB}}/l_{b,\mathrm{PNB}} = 14.6$ — a Kuhn segment of PNB includes ca. 14.6 chemical bonds. Noting that there are three chemical bonds in a PLA repeat unit, it is possible to calculate the number of repeat units per Kuhn length for PLA $p_{K,\mathrm{PLA}} = 7.84/3 \approx 2.6$ repeat units. Similarly, for PNB with five chemical bonds per repeat unit $b_{K,\mathrm{PNB}}$ includes $p_{K,\mathrm{PNB}} = 14.6/5 \approx 2.92$ repeat units.

The number of monomers in a bottlebrush molecule is dominated by contribution from the side chains, so we will calculate a length scale based on the side chain monomers. Recall from Section 2.4 that we represent the side chains using a Kremer-Grest (KG) model with no bending penalty. Equating the Kuhn length of PLA $b_{K,\mathrm{PLA}}$ to the Kuhn length $b_{K,\mathrm{KG}} = 1.795\sigma$[108] of a KG chain, we obtain $\sigma = 0.67$ nm, which serves as the length scale for our system.

A side chain of N_{sc} beads has a contour length $L_{sc} = r_{\max}(N_{sc}-1)$ (see eqn (1)), which contains $L_{sc}/b_{K,\mathrm{KG}}$ Kuhn segments. Mapping to PLA at the level of Kuhn segments, N_{sc} beads represent $n_{sc} = p_{K,\mathrm{PLA}} \times L_{sc}/b_{K,\mathrm{KG}} = 2.17(N_{sc}-1)$ chemical repeat units of PLA.

An analogous calculation for PNB to determine n_{bb} would be incorrect due to inconsistent level of discretization. A Kuhn segment of PLA includes ca. 7.84 chemical bonds, but that of PNB includes 14.6 chemical bonds. Here we encounter two different length scales, corresponding to two different species of polymers exhibiting different stiffness. We choose to work in terms of the length scale obtained based on a PLA repeat unit.

In Section 2.4 we describe PNB as being modeled by a KG chain with bending potential $k_b = 0.5$, whose Kuhn length $b'_{K,\mathrm{KG}} = 2.019\sigma$.[108] If this is to map to a PNB chain with 14.6 chemical bonds per Kuhn length while maintaining the local packing density as well as consistent discretization throughout, the number of PNB repeat units need to be $n_{bb} = (7.84/14.6) \times p_{K,\mathrm{PNB}} \times (L_{bb}/b'_{K,\mathrm{KG}}) \approx 0.5 \times p_{K,\mathrm{PNB}} \times (L_{bb}/b'_{K,\mathrm{KG}}) = 1.1(N_{bb}-1)$, where $L_{bb} = r_{\max}(N_{bb}-1)$ is the backbone contour length. This approximate factor of half leads us to introduce a bending penalty on the backbone; in hindsight, removing this bending penalty has minimal quantitative effect.

The molecular weights of PLA and PNB repeat units being 74.56 Da and 124 Da, respectively, $M_{sc} = 74.56 \times n_{sc} = 161.8(N_{sc}-1)$ Da and $M_{bb} = 124 \times n_{bb} = 134.6(N_{bb}-1)$ Da; the total molecular weight (as dictated by chemistry with a grafting density of unity) $M = M_{bb}+n_{bb} \times M_{sc} = 134.6(N_{bb}-1)+161.8N_{sc}N_{bb}$ Da. The mapping parameters derived above are summarized in Table 1.

3 Results and discussion

We show that experiment and simulation, upon appropriate parameterization of the latter, can exhibit quantitative matching. This matching relies on experimental data that is sufficiently sensitive to reflect differences in the synthesized bottlebrush structure, for which we primarily use intrinsic viscosity. We interpret this data in the context of both conceptual arguments as well as the corresponding simulation, which provides a direct glimpse at molecular conformations adapted by these bottlebrush molecules. This provides a direct characterization of molecular shape and size, showing that an increase in backbone length results in a change from a star-like structure to a short cylinder, and finally to a flexible cylinder.

3.1 Bottlebrush Synthesis

Bottlebrushes were synthesized by ring opening polymerization (ROP) of *rac*-lactide utilizing a 1,8-diazabicyclo[5.4.0]undec-7-ene (DBU) catalyst, followed by the ring opening metathesis poly-

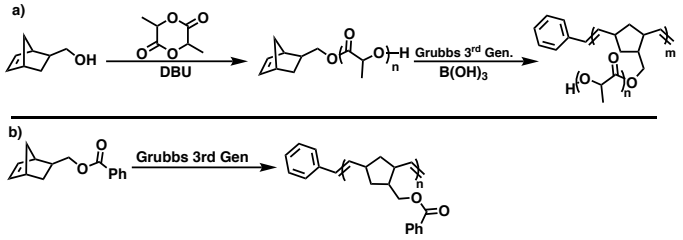

Scheme 1 (a) Synthetic scheme for the one pot synthesis of PLA bottlebrush polymers. (b) Synthetic scheme for the synthesis of linear poly(5-norbornene-2-(methylbenzoate)).

merization (ROMP) of norbornene terminated macromonomer with third generation Grubbs catalyst (see Scheme 1).[89,109,110] Boric acid was used as a quenching agent for the ROP catalyst to perform the *graft-through* process without isolating the macromonomers.[48] Molecular weight of the bottlebrush polymers were determined based on macromonomer to initiator ratio and macromonomer conversion determined by RI-GPC.[48]

Three series of bottlebrushes were made: (i) long backbone sweep, spanning backbone DP (n_{bb}) from 10 to 1000 at side chain DP (n_{sc}) of 70 polylactic acid (PLA) repeat units (see Table 2); (ii) short backbone sweep, spanning n_{bb} from 10 to 2000 at $n_{sc} = 30$ PLA repeat units (see Table 3); and (iii) side chain sweep, spanning n_{sc} from 5 to 100 at $n_{bb} = 200$ (see Table 4). The spacings between the samples were increased exponentially for each of the above sweeps. Linear poly(5-norbornene-2-(methyl benzoate)) samples with DP ranging from 10 to 1000 were also synthesized via ROMP (see Table 5). GPC traces are provided as ESI†. The broadening of the molecular weight with n_{bb} is likely caused by the slow decomposition of the ruthenium complex.

3.2 Intrinsic viscosity

Intrinsic viscosity measurements were performed on a series of model bottlebrush polymers, as described in Section 2.3. We plot these experimental results (filled symbols) as a function of molecular weight M in Fig. 2, for bottlebrush molecules with $M_{sc} = 2237$ Da and $= 5220$ Da, and also linear PNB. The simulation data for linear PNB fits a power-law behavior $[\eta] \sim M^{0.73}$, in close agreement with the Flory-Fox relationship consistent with the expectation for a coil in a good solvent. The corresponding experimental data yields $[\eta] \sim M^{0.67}$, which is slightly lower than the simulation result. Note that this is expected, as the simulation result pertains to a solution in athermal condition. The bottlebrush measurements are consistent with previous literature,[25,111,112] showing significant deviations from the Flory-Fox result at low M, with very little initial change in $[\eta]$ with increasing M. We attribute this to the star-like nature of the low-M_{bb} bottlebrush, with additional backbone monomers increasing the local density of branches rather than the overall aspect ratio of the molecule. This corresponds to molecular simulation snapshots in the same low-n_{bb} limit of Fig. 3. At high M, however, there is once again an increase in the intrinsic viscosity as added n_{bb} reflects an increase in the molecular structure. Interestingly, this system exhibits significant differences in $[\eta]$ values as molecular structure is changed by either adding to the backbone or branches for a given molecular weight, and thus allows us to distinguish the architecture of the synthesized molecule via characterization. However, many of the differences in $[\eta]$ versus M become less pronounced upon plotting instead versus M_{bb} in the limit of high M_{bb} (Fig. 2 (b)). This reflects the increased importance of the backbone length in this limit, which is the primary quantity establishing the molecular size as captured by $[\eta]$. We interpret the small but non-negligible changes due to M_{sc} as primarily reflecting the effect of side-chain "stiffening" of the molecular contour.

We show that simulation results for the intrinsic viscosity $[\eta]$ are in quantitative agreement with the experimental data. Because this value is sensitive to molecular architecture, this matching between simulation and experiment shows that coarse-grained bead-spring simulations are capable of capturing the essential physics associated with bottlebrush polymer conformations; namely, the structure can be explained using the conceptual arguments about how the "size" of the coil changes with M without invoking specific chemistry. This matching also provides a snapshot of typical bottlebrush structures, for which we show a number of examples in Fig. 3. These snapshots were generated using the molecular visualization package Ovito.[113] We note that, for a bottlebrush architecture, the increase in length of the backbone results in a transition from a roughly-star-like polymer, to an elongated structure (around $n_{bb} = 87$ for both n_{sc} shown), and then finally to a coil-like shape. These transitions are subtly different for each different value of n_{sc}, which is especially apparent around $n_{bb} = 87$ and 175, which show that the longer branches lead to a marginally "stiffer"-appearing structure. In subsequent sections, we will further explore these bottlebrush shape transitions in a quantitative fashion.

We plot the simulation behavior of $[\eta]$ as a function of the overall molecular weight M and backbone molecular weight M_{bb} for a number of different side chain lengths M_{sc} in Fig. 4, as well as for a linear molecule. Notably, we observe the general trends associated with the regimes plotted in the experimental comparison in Fig. 2; the initial weak dependence on M associated with a star-like geometry shows an increase in $[\eta]$ commensurate with the increase in the branch length, because the star-like structure is thus larger. The upswing in the intrinsic viscosity occurs also at a larger value of M for longer M_{sc}, because the backbone needs to be sufficiently long to register an extension of the bottlebrush structure beyond the length of the side chains. The terminal scaling exponent is plotted as ν_v versus the side-chain M_{sc}, showing that there is a small but non-negligible increase due to the side-chain induced stiffening of the bottlebrush structure. This is consistent with the experimental scaling values shown in Fig. 2 and also with prior experimental work on polystyrene bottlebrushes.[112] In case of very high molecular weight side chains, $[\eta]$ and ν_v were reported to decrease with increase in M_{bb} and M_{sc}, respectively.[114,115] Side chains of such high molecular weights are not considered here as they are beyond our current experimental and computational capabilities.

Theory		Macromonomer			Bottlebrush			
n_{sc}	n_{bb}	M_n (g/mol)[a]	n_{sc}	M_w/M_n	$M_n \times 10^{-3}$ (g/mol)[b]	$M_n \times 10^{-3}$ (g/mol)[c]	M_w/M_n	Norbornene conversion (%)[d]
70	10	5200	70.4	1.06	52	44.9	1.06	>98
70	19	5200	70.4	1.06	100	63.3	1.06	>98
70	37	5200	70.4	1.06	194	94.7	1.04	>98
70	72	5200	70.4	1.06	375	152	1.04	>98
70	139	5200	70.4	1.06	724	254	1.05	>98
70	268	5200	70.4	1.06	1400	496	1.04	>98
70	518	5200	70.4	1.06	2700	918	1.13	>98
70	1000	5200	70.4	1.06	5200	1300	1.13	>98

[a] GPC molecular weight against PLA calibration standard
[b] Conversion molecular weight = GPC M_n for brush $\times$ conversion of macromonomer
[c] GPC molecular weight against PS calibration standard
[d] Calculated from GPC area

Table 2 Bottlebrush polymers used in backbone sweep with long side chains.

Theory		Macromonomer			Bottlebrush			
n_{sc}	n_{bb}	M_n (g/mol)[a]	n_{sc}	M_w/M_n	$M_n \times 10^{-3}$ (g/mol)[b]	$M_n \times 10^{-3}$ (g/mol)[c]	M_w/M_n	Norbornene conversion (%)[d]
30	10	2300	30.4	1.09	23.2	23.2	1.06	>98
30	19	2300	30.4	1.09	44.8	34.8	1.05	>98
30	37	2300	30.4	1.09	86.4	52.3	1.04	>98
30	72	2300	30.4	1.09	167	84.7	1.04	>98
30	139	2300	30.4	1.09	322	151	1.04	>98
30	268	2300	30.4	1.09	622	281	1.09	>98
30	518	2300	30.4	1.09	1200	539	1.09	>98
30	1000	2300	30.4	1.09	2320	928	1.18	>98
30	2000	2300	30.4	1.09	4640	1360	1.29	>95

[a] GPC molecular weight against PLA calibration standard
[b] Conversion molecular weight = GPC M_n for brush $\times$ conversion of macromonomer
[c] GPC molecular weight against PS calibration standard
[d] Calculated from GPC area

Table 3 Bottlebrush polymers used in backbone sweep with short side chains.

Theory		Macromonomer			Bottlebrush			
n_{sc}	n_{bb}	M_n (g/mol)[a]	n_{sc}	M_w/M_n	$M_n \times 10^{-3}$ (g/mol)[b]	$M_n \times 10^{-3}$ (g/mol)[c]	M_w/M_n	Norbornene conversion (%)[d]
18	200	1500	19	1.11	297	158	1.04	>98
25	200	2000	27	1.09	411	186	1.03	>98
36	200	2900	38	1.08	578	220	1.03	>98
51	200	3900	53	1.07	785	270	1.04	>98
72	200	5200	71	1.06	1050	327	1.04	>98
103	200	7400	101	1.05	1477	399	1.04	>98

[a] GPC molecular weight against PLA calibration standard
[b] Conversion molecular weight = GPC M_n for brush $\times$ conversion of macromonomer
[c] GPC molecular weight against PS calibration standard
[d] Calculated from GPC area

Table 4 Bottlebrush polymers used in side chain sweep.

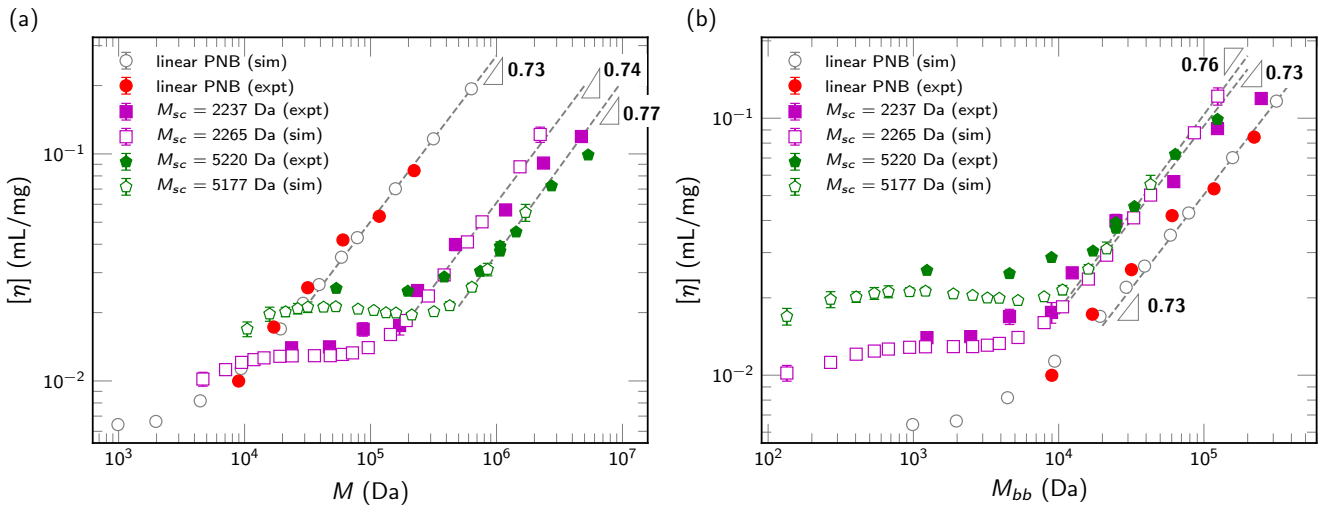

Fig. 2 Intrinsic viscosity $[\eta]$ as a function of bottlebrush molecular weight. Filled symbols denote experimental measurements at 30 °C and unfilled symbols denote simulation results. The dashed lines are fits to the simulation data. (a) $[\eta]$ vs. M for both experimental and simulation data; (b) $[\eta]$ vs. M_{bb} for both experimental and simulation data.

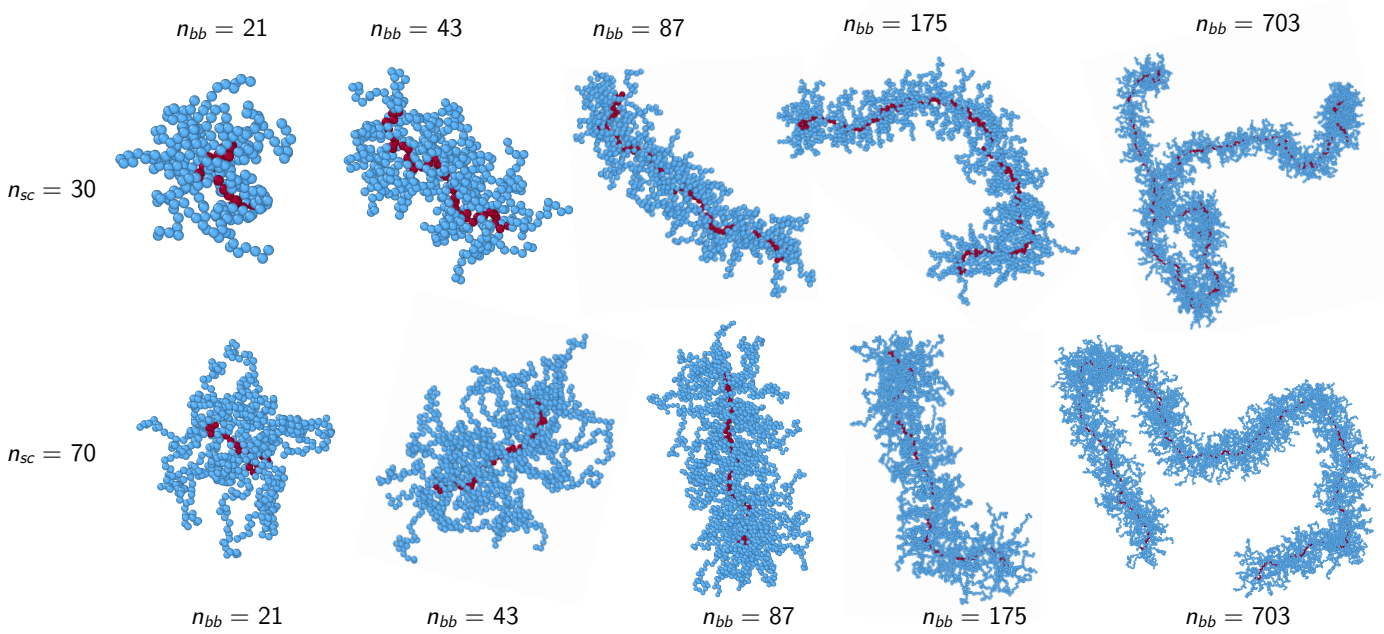

Fig. 3 Simulation snapshots of a bottlebrush with varying backbone lengths for side chain DP 30 and 70.

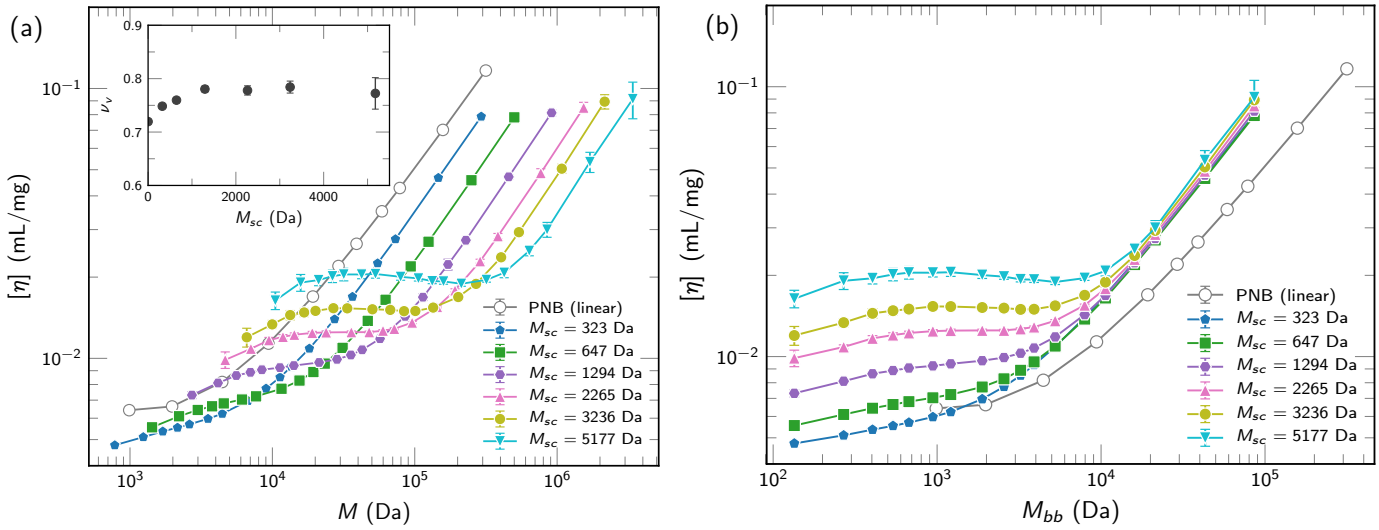

Fig. 4 Intrinsic viscosity as a function of bottlebrush molecular weight M (a) and backbone molecular weight (M_{bb}) for different side chain molecular weights (M_{sc}). Solid lines are intended to guide the eye. *Inset.* Exponent (ν_v) calculated from a power-law fit of $[\eta]$ *vs.* M as a function of M_{sc}.

n_{bb}	$M_n \times 10^{-3}$ (theory) (g/mol)	$M_n \times 10^{-3}$ (GPC)[a] (g/mol)	M_w/M_n
10	2.28	2.26	1.16
19	4.41	4.50	1.21
37	8.51	8.97	1.05
72	16.4	17.1	1.06
139	31.7	31.7	1.04
268	61.2	60.4	1.06
518	118	117	1.09
1000	228	222	1.17

[a] GPC molecular weight against PS calibration standard.

Table 5 Samples used for linear poly(5-norbornene-2-(methylbenzoate)) sweep.

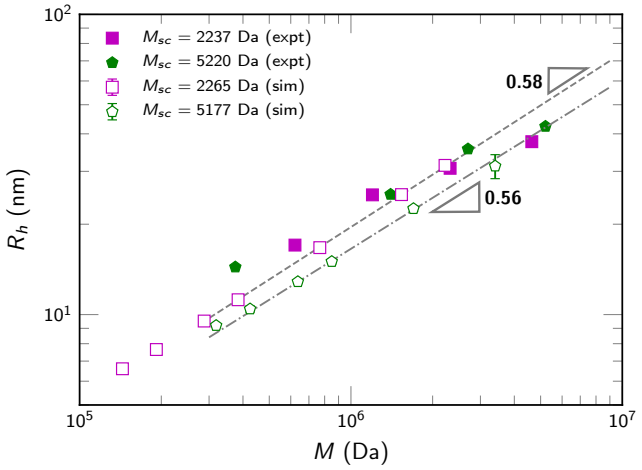

Fig. 5 Hydrodynamic radius as a function of bottlebrush molecular weight. Filled symbols denote experimental measurements and unfilled symbols denote simulation results. The dashed lines are fits to the simulation data.

3.3 Hydrodynamic radius

Hydrodynamic radius is a quantity related to intrinsic viscosity, and can be measured in dynamic light scattering measurements. These provide another measure of the molecular size by capturing the Stokes drag radius of an equivalent sphere undergoing the same center-of-mass diffusion as the bottlebrush. We plot this in Fig. 5, which shows that for large M for both values of M_{sc} tested there is nearly quantitative agreement between simulation and experiment. In contrast to intrinsic viscosity, however, both the simulation predictions and the measured values are less sensitive to the molecular changes (i.e. M_{sc}) and thus provide less insight into dilute solution bottlebrush conformation.

We plot the simulation behavior of R_h as a function of the overall molecular weight M and backbone molecular weight M_{bb} in Fig. 6, for a number of side chain lengths M_{sc}. The main changes in R_h occur as the backbone length is increased, which reflects the increasing length and thus size of the overall polymer. A significantly smaller difference is observed between different side chain lengths, similar to the intrinsic viscosity observations, though these differences remain small even at low M_{bb}. This is consistent with the Monte Carlo results of Yethiraj.[54]

We use R_h to show that there are only small differences in geometric parameters due to changes in temperature, which we plot for a few characteristic values of M_{sc} as a function of T in Fig. 7 (a). Indeed, relatively small changes in R_h are observed even over a large range of temperatures ($0\,^\circ\mathrm{C} < T < 90\,^\circ\mathrm{C}$). Comparison with simulations suggests that this means we remain well above the θ-temperature and are in the good solvent regime. We plot in Fig. 7 (b) the hydrodynamic radius R_h as a function of temperature (in units of ε/k_B). We note large changes in bottlebrush size as we transition from a θ-temperature ($T = 1.5\varepsilon/k_B$) to the athermal limit (point shown, $T \to \infty$). These changes in bottlebrush size, however, occur relatively close to the θ-temperature, whereas in the athermal limit, we see only small deviations in terms of size. Furthermore, these athermal limit sizes are more

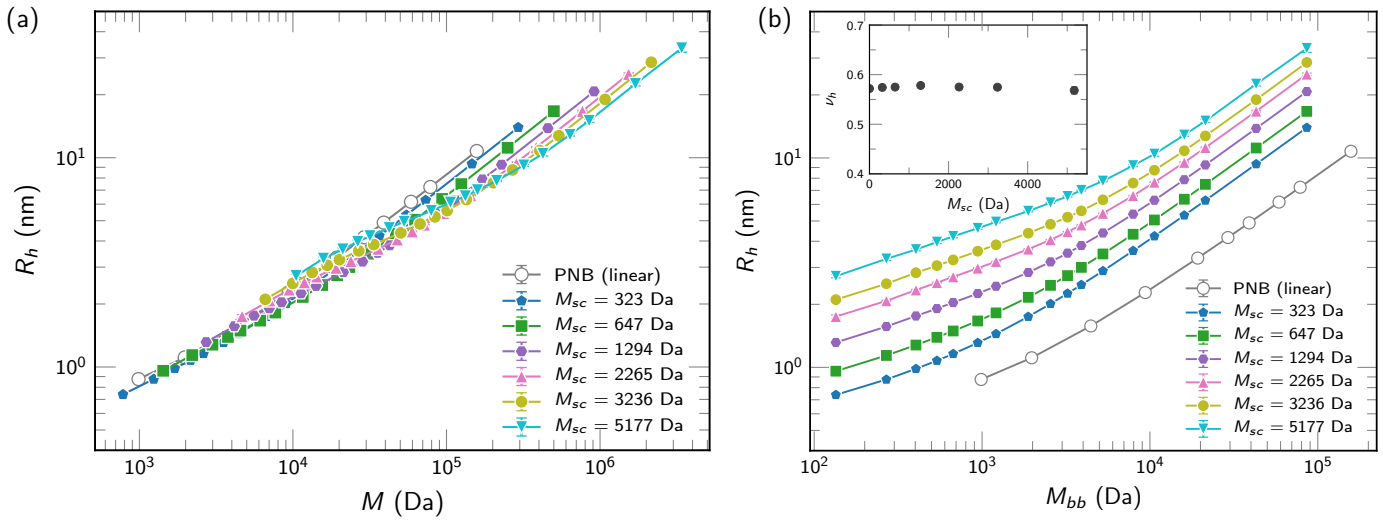

Fig. 6 Hydrodynamic radius as a function of bottlebrush molecular weight M (a) and backbone molecular weight M_{bb} (b) for different side chain molecular weights (M_{sc}). Solid lines are intended to guide the eye. *Inset.* Exponent (ν_h) calculated from a power-law fit of R_h *vs.* M_{bb} as a function of M_{sc}.

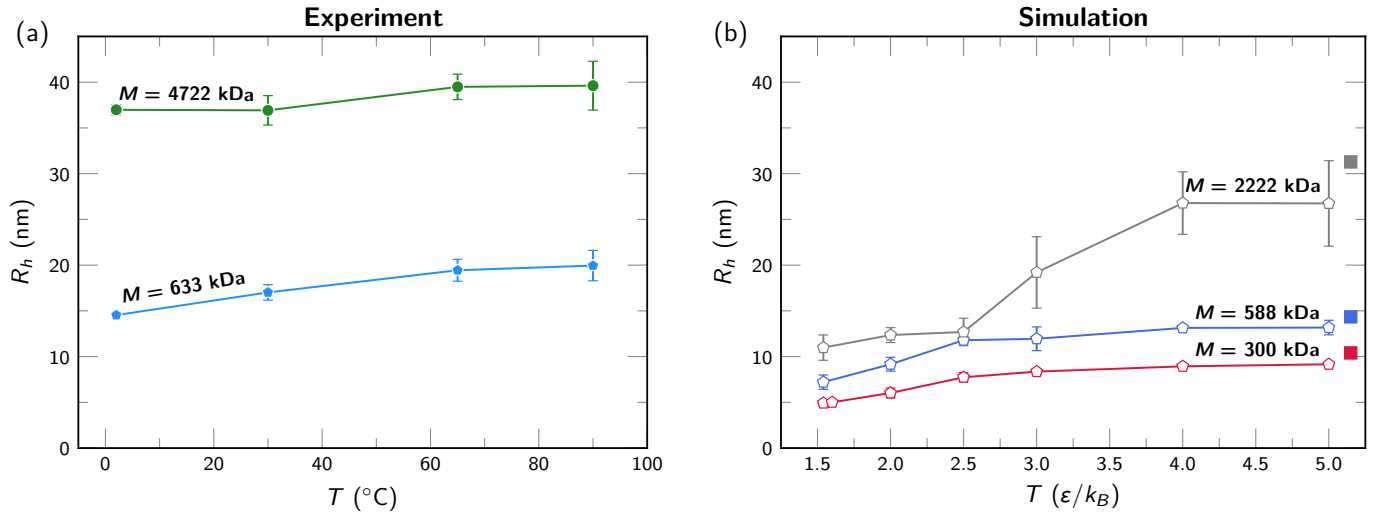

Fig. 7 Hydrodynamic radius R_h as a function of temperature for bottlebrushes: (a) experiment (b) simulation. The side chain molecular weight is 2237 Da for all cases. In (b) the filled squares indicate R_h in the athermal limit. Solid lines are intended to guide the eye.

consistent with the measured R_h in experiment. In the supplemental information, we show slight differences in $[\eta]$ due to temperature, however these are also small with respect to architectural changes in the bottlebrush polymer.

3.4 Radius of gyration and backbone contributions

Intrinsic viscosity and hydrodynamic radius reflect near-equilibrium dynamic quantities, and are calculated using the Kirkwood approximation from simulation. In contrast, the radius of gyration R_g is a purely structural quantity that can be used to understand aspects of the internal architectural features such as the behavior of the branches and backbones separately. This is only possible in simulation, but favorable, quantitative comparison in intrinsic viscosity and R_h give us confidence in using simulation to probe these features.

In Fig. 8 (a), we plot the radius of gyration for a series of bottlebrush molecules of varying M_{bb} and M_{sc}. Similar features are seen in the quantity R_g^2 as in $[\eta]$, with a regime where the "star-like" molecules at low M_{bb} do not increase rapidly with added M_{bb} because the addition of branches to make a more-armed star is the main effect of adding another backbone monomer. To show how this occurs, we also plot the R_g^2 of the backbone specifically in Fig. 8 (a), and show that this value is significantly smaller than the overall molecule size at $M_{bb} < 10^4$ Da. However, at large values of M_{bb} the backbone begins to track very closely with the overall size of the overall R_g^2, meaning that additional M_{bb} is the main contributor to the size trends of the molecule. We further note that the increase in side-chain length can affect the backbone in this limit, with a scaling exponent as shown in the inset of Fig. 8 (a). This exponent increases from the ideal value $2\nu \approx 1.2$ to a larger scaling value indicative of the stiffening effect of the long side-chains. Nevertheless, this remains significantly less than the rod-like limit $2\nu < 2$ reflecting the wormlike structures seen in Fig. 3. Additional plots for radius of gyration as well as for R_g/R_h are provided as ESI†.

We can also plot similar $R_{g,sc}^2$ quantities for the side-chains as a function of the polymer architectural features. In particular, we show in Fig. 8 (b) both $R_{g,sc}^2$ and the end-to-end distance $R_{ee,sc}^2$ as a function of the side-chain length M_{sc} for a number of values of M_{bb}. Two scaling observations are observed; first, the value of the backbone M_{bb} does not have a large effect on the conformational properties of the side-chains, which we attribute to the long bottlebrush backbones considered, with a given side-chain existing in an environment far from the chain end. Second, there is a super-linear scaling of R_g^2 (both measures) with M_{sc}, indicating that the side-chain does not undergo a random walk and is indeed slightly stretched due to the steric interactions with neighboring chains. We attribute the deviation in the scaling exponents for $R_{g,sc}^2$ and $R_{ee,sc}^2$ to the relatively short length of the side chains, which are unlikely to have reached their respective asymptotic limits.

3.5 Bottlebrush shape

Dynamic quantities such as R_h and $[\eta]$ provide straightforward ways to compare between computation and experiment, and the structural measure of R_g can be compared via scattering methods not pursued in this investigation. Interpretation of these accessible quantities, however, are related to the shape of the bottlebrush. Shape information has been investigated in part by prior works using theory[62,63] and neutron scattering,[35] and has also been implicated in explaining the low viscosity of bottlebrush melts.[116] However, full architectural information from simulation provides the opportunity to directly characterize shape using a number of measures: (i) *asphericity*, which quantifies the deviation of a shape from a sphere, and (ii) *prolateness*, which quantifies the degree of oblateness or prolateness of a shape.

The asphericity Δ is defined as[117]

$$\Delta = \frac{3}{2}\frac{\sum_{i=1}^{3}\left(\lambda_i - \bar{\lambda}\right)^2}{\left[\sum_{i=1}^{3}\lambda_i\right]^2}. \quad (2)$$

Here λ_i are the eigenvalues of the gyration tensor and $\bar{\lambda}$ denotes their mean. This value has the bounds $0 \leq \Delta \leq 1$, such that if the monomers of a bottlebrush are distributed isotropically around its center-of-mass, Δ vanishes as the shape resembles a sphere. A non-zero value of Δ indicates an anisotropic distribution of monomers. We plot the average asphericity $\langle\Delta\rangle$ as a function of M_{bb} for a number of side chain molecular weights M_{sc} in Fig. 9 (a), and include snapshots to highlight characteristic shapes and their corresponding values of $\langle\Delta\rangle$. There is also a comparison with a linear coil (open symbols), which has a well-established asphericity of ca. 0.42.[117,118]

We observe shape features consistent with the interpretations of $[\eta]$, R_h, and R_g. At low values of M_{bb}, there is a decrease in asphericity as the molecule transitions from a two-armed star (with an asphericity typical of a short polymer chain) to a star-like polymer (second snapshot in Fig. 9 (a)). This star-like molecule begins to elongate approximately as M_{bb} increases beyond the M_{sc}, leading to a marked increase in the value of $\langle\Delta\rangle$. Bottlebrushes with the same M_{bb} but shorter side chains have higher aspect ratio, so $\langle\Delta\rangle$ increases with M_{sc} in this region. A similar trend in $\langle\Delta\rangle$ with M_{sc} can be seen in prior simulation studies as well.[51,119] The stiffness of this elongated shape causes it to extend beyond the asphericity of a random coil, and then decrease to the random coil limit at large M_{bb}. This latter region is consistent with the observations that the intrinsic viscosity and R_h exhibit scaling exponents ν_v and ν_h slightly larger than the swollen-coil values.

The prolateness Σ can also be used to characterize the shape:[117]

$$\Sigma = 4\,\frac{\prod_{i=1}^{3}\left(\lambda_i - \bar{\lambda}\right)}{\left[\frac{2}{3}\sum_{i=1}^{3}\left(\lambda_i - \bar{\lambda}\right)^2\right]^{3/2}}, \quad (3)$$

where Σ has the bounds $-1 \leq \Sigma \leq 1$, and captures the nature of the anisotropy by a non-zero value. Oblate shapes have $\Sigma < 0$ and prolates have $\Sigma > 0$. We plot the average prolateness $\langle\Sigma\rangle$ as a function of M_{bb} for a number of values of M_{sc} in Fig. 9 (b), and can directly compare to the asphericity observations in Fig. 9 (a). There is a similar trend in the overall values, with an approach to spherical $\langle\Sigma\rangle \to 0$ at a similar M_{bb} at the same point as in $\langle\Delta\rangle$ and values that approach the linear chain predictions at high M_{bb}. All of the chains exhibit prolate geometries, including the linear

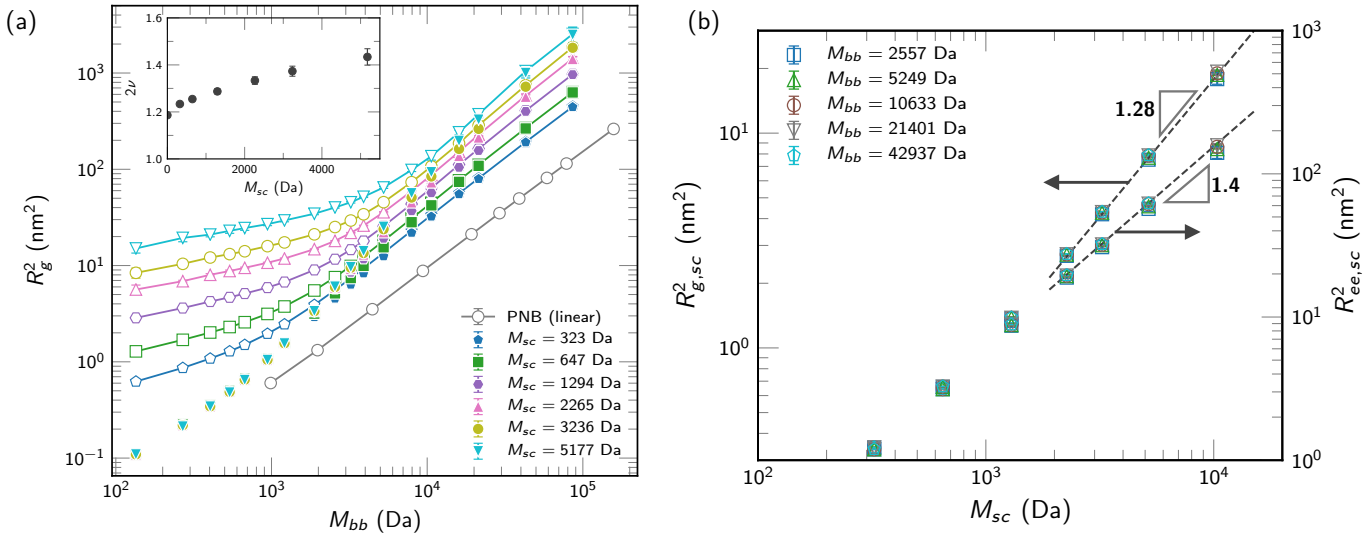

Fig. 8 (a) Mean-squared radius of gyration as a function of backbone molecular weight M_{bb} for different side chain molecular weights (M_{sc}). Filled symbols represent the backbone mean-squared radius of gyration ($R_{g,bb}^2$), whereas the unfilled symbols represent that of an entire bottlebrush. Solid lines are intended to guide the eye. *Inset.* Exponent (2ν) calculated from a power-law fit of $R_{g,bb}^2$ *vs.* M_{bb} as a function of M_{sc}. (b) Mean-squared radius of gyration $R_{g,sc}^2$ and mean-squared end-to-end distance $R_{ee,sc}^2$ of side chains as a function of side chain molecular weight M_{sc} for different backbone molecular weights (M_{bb}). Dashed lines are power-law fits to the high M_{sc} range of the data.

chain; the latter is expected from both the theoretical and simulation literature.[117,118,120]

These established measures of molecular shape provide information that is consistent with experimental observations, and provide further insight by confirming their interpretation. Furthermore, these shape measures provide a quantitative measure to reinforce the observation of individual simulation snapshots; namely, as a bottlebrush backbone increases in length, it transitions from a spherical star-like conformation, to a short cylinder, and finally to a flexible cylinder that exhibits the limiting behavior of a semiflexible coil. This will be useful as the architecture or chemical nature of the brush becomes more complicated, and molecular shapes become more complicated.

4 Conclusions

In this manuscript, we show that the combined use of precise synthesis, intrinsic viscosity measurements, light scattering, and parameterized computer simulations can provide insight into the conformational properties of dilute bottlebrush polymers. We use a set of model bottlebrushes to show that intrinsic viscosity is an accessible and *sensitive* property that can reflect architectural differences in e.g. backbone length and branch length. Intrinsic viscosity also suggests how geometry changes upon increasing the backbone length for a given branch length, with changes from a star-like structure, to an extended rod, and finally to a coil-like chain.

We parameterize the structure of the bottlebrush using molecular arguments to obtain a coarse-grained simulation model that exhibits near-quantitative matching to experimental measurements of intrinsic viscosity and hydrodynamic radius. The molecular information in these simulations provide access to further structural quantities, in particular those describing sub-molecule structures and molecular shape. For the former, we focus on how the radius of gyration of the overall molecule is related to the backbone and side-chain radii of gyration separately. This shows two physical limits, one where the side-chains dominate the overall structural measure, and the other in the long backbone limit where this length sets the molecular size. Finally, we characterize shape using asphericity and prolateness, which we use as quantitative measures to explore the geometric contributions to bottlebrush structures and the experimentally-measured values.

This model provides a platform to understand the shape and structure of dilute bottlebrushes, in the context of a wide number of variations beyond what we consider in this manuscript. For example, grafting density and varying-width bottlebrushes are structural variations of interest, along with block bottlebrush chemistries. Such a model can also be potentially adapted for studying bottlebrushes with varying thickness[36,48] (e.g. cone-shaped or tapered bottlebrushes) as well as multi-block bottlebrushes (with additional parameters accounting for differences in interaction between the blocks). We expect that combined simulation-experimental model development will enable predictive *in silico* methods that can address the ever-expanding parameter space associated with this emerging class of macromolecules. Finally, we anticipate that further coarse-graining approaches may be capable of considering increasingly complex systems such as non-dilute solutions in- and out-of-equilibrium, or in bottlebrush self-assembly.

Conflicts of interest

There are no conflicts to declare.

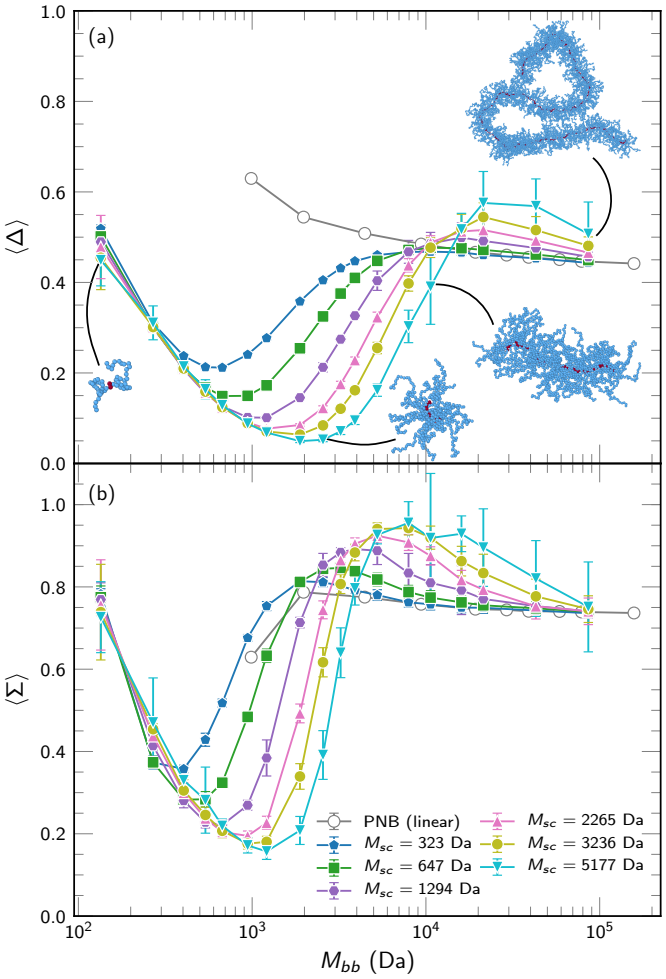

Fig. 9 Asphericity (a) and prolateness (b) of bottlebrushes as a function of backbone molecular weight M_{bb} for different side chain molecular weights (M_{sc}). Solid lines are intended to guide the eye.

Acknowledgements

This work was supported by National Science Foundation under DMREF Award Number DMR-1727605. The authors thank Ying Diao, Bijal Patel, Ching-Wei Lee, Jaimie Kurtz and Michael Samp for intellectual discussions regarding this work.

References

1 S. Namba, Y. Tsukahara, K. Kaeriyama, K. Okamoto and M. Takahashi, *Polymer*, 2000, **41**, 5165–5171.

2 S. S. Sheiko, B. S. Sumerlin and K. Matyjaszewski, *Prog. Polym. Sci.*, 2008, **33**, 759–785.

3 J. Rzayev, *ACS Macro Lett.*, 2012, **1**, 1146–1149.

4 F. Sun, S. S. Sheiko, M. Möller, K. Beers and K. Matyjaszewski, *J. Phys. Chem. A*, 2004, **108**, 9682–9686.

5 H. Xu, F. C. Sun, D. G. Shirvanyants, M. Rubinstein, D. Shabratov, K. L. Beers, K. Matyjaszewski and S. S. Sheiko, *Adv. Mater.*, 2007, **19**, 2930–2934.

6 K. J. Arrington, S. C. Radzinski, K. J. Drummey, T. E. Long and J. B. Matson, *ACS Appl. Mater. Interfaces*, 2018, **10**, 26662–26668.

7 H.-I. Lee, J. R. Boyce, A. Nese, S. S. Sheiko and K. Matyjaszewski, *Polymer*, 2008, **49**, 5490–5496.

8 H.-I. Lee, J. Pietrasik, S. S. Sheiko and K. Matyjaszewski, *Prog. Polym. Sci.*, 2010, **35**, 24–44.

9 W. Gu, J. Huh, S. W. Hong, B. R. Sveinbjörnsson, C. Park, R. H. Grubbs and T. P. Russell, *ACS Nano*, 2013, **7**, 2551–2558.

10 R. Verduzco, X. Li, S. L. Pesek and G. E. Stein, *Chem. Soc. Rev.*, 2015, **44**, 2405–2420.

11 T. Pelras, C. S. Mahon and M. Müllner, *Angew. Chem. Int. Ed.*, 2018, **57**, 6982–6994.

12 B. R. Sveinbjörnsson, R. A. Weitekamp, G. M. Miyake, Y. Xia, H. A. Atwater and R. H. Grubbs, *Proc. Natl. Acad. Sci. U.S.A.*, 2012, **109**, 14332–14336.

13 Y. Saito, M. Kikuchi, Y. Jinbo, A. Narumi and S. Kawaguchi, *Macromolecules*, 2015, **48**, 8971–8979.

14 A. L. Liberman-Martin, C. K. Chu and R. H. Grubbs, *Macromol. Rapid Commun.*, 2017, **38**, 1700058.

15 A. Aluculesei, A. Pipertzis, V. A. Piunova, G. M. Miyake, G. Floudas, G. Fytas and R. H. Grubbs, *Macromolecules*, 2015, **48**, 4142–4150.

16 L.-H. Cai, T. E. Kodger, R. E. Guerra, A. F. Pegoraro, M. Rubinstein and D. A. Weitz, *Adv. Mater.*, 2015, **27**, 5132–5140.

17 M. Vatankhah-Varnoosfaderani, W. F. M. Daniel, A. P. Zhushma, Q. Li, B. J. Morgan, K. Matyjaszewski, D. P. Armstrong, R. J. Spontak, A. V. Dobrynin and S. S. Sheiko, *Adv. Mater.*, 2016, **29**, 1604209–7.

18 M. Vatankhah-Varnosfaderani, W. F. M. Daniel, M. H. Everhart, A. A. Pandya, H. Liang, K. Matyjaszewski, A. V. Dobrynin and S. S. Sheiko, *Nature*, 2017, **549**, 497–501.

19 M. Vatankhah-Varnosfaderani, A. N. Keith, Y. Cong, H. Liang, M. Rosenthal, M. Sztucki, C. Clair, S. Magonov, D. A. Ivanov, A. V. Dobrynin and S. S. Sheiko, *Science*, 2018, **359**, 1509–1513.

20 H. Liang, S. S. Sheiko and A. V. Dobrynin, *Macromolecules*, 2018, **51**, 638–645.

21 F. Horkay, *J. Polym. Sci., Part B: Polym. Phys.*, 2012, **50**, 1699–1705.

22 M. Kornreich, E. Malka-Gibor, A. Laser-Azogui, O. Doron, H. Herrmann and R. Beck, *Soft Matter*, 2015, **11**, 5839–5849.

23 T. Birshtein, O. Borisov, Y. Zhulina, A. Khokhlov and T. Yurasova, *Polym. Sci. U.S.S.R*, 1987, **29**, 1293–1300.

24 G. H. Fredrickson, *Macromolecules*, 1993, **26**, 2825–2831.

25 Y. Tsukahara, S. Kohjiya, K. Tsutsumi and Y. Okamoto, *Macromolecules*, 1994, **27**, 1662–1664.

26 M. Wintermantel, K. Fischer, M. Gerle, R. Ries, M. Schmidt, K. Kajiwara, H. Urakawa and I. Wataoka, *Angew. Chem., Int. Ed. Engl.*, 1995, **34**, 1472–1474.

27 M. Wintermantel, M. Gerle, K. Fischer, M. Schmidt, I. Wataoka, H. Urakawa, K. Kajiwara and Y. Tsukahara, *Macromolecules*, 1996, **29**, 978–983.

28 S. Kawaguchi, K. Akaike, Z.-M. Zhang, H. Matsumoto and K. Ito, *Polym. J.*, 1998, **30**, 1004–1007.

29 D. Vlassopoulos, G. Fytas, B. Loppinet, F. Isel, P. Lutz and H. Benoit, *Macromolecules*, 2000, **33**, 5960–5969.

30 Y. Nakamura, Y. Wan, J. W. Mays, H. Iatrou and N. Hadjichristidis, *Macromolecules*, 2000, **33**, 8323–8328.

31 S. Rathgeber, T. Pakula, A. Wilk, K. Matyjaszewski and K. L. Beers, *J. Chem. Phys.*, 2005, **122**, 124904–14.

32 M. Zhang and A. H. E. Müller, *J. Polym. Sci. A Polym. Chem.*, 2005, **43**, 3461–3481.

33 P. E. Theodorakis, W. Paul and K. Binder, *Europhys. Lett.*, 2009, **88**, 63002.

34 P. E. Theodorakis, W. Paul and K. Binder, *J. Chem. Phys.*, 2010, **133**, 104901.

35 S. L. Pesek, X. Li, B. Hammouda, K. Hong and R. Verduzco, *Macromolecules*, 2013, **46**, 6998–7005.

36 S. C. Radzinski, J. C. Foster, R. C. Chapleski, D. Troya and J. B. Matson, *J. Am. Chem. Soc.*, 2016, **138**, 6998–7004.

37 C. R. López-Barrón, A. H. Tsou, J. R. Hagadorn and J. A. Throckmorton, *Macromolecules*, 2018, **51**, 6958–6966.

38 J. Yuan, A. Müller, K. Matyjaszewski and S. Sheiko, in *Molecular Brushes*, Elsevier, 2012, pp. 199–264.

39 M. Müllner, K. Yang, A. Kaur and E. J. New, *Polym. Chem.*, 2018, **9**, 3461–3465.

40 D. G. Angelescu and P. Linse, *Macromolecules*, 2013, **47**, 415–426.

41 E. Flikkema, A. Subbotin and G. ten Brinke, *J. Chem. Phys.*, 2000, **113**, 7646–7651.

42 M. Kikuchi, T. Mihara, Y. Jinbo, Y. Izumi, K. Nagai and S. Kawaguchi, *Polym. J.*, 2007, **39**, 330–341.

43 I. M. Storm, M. Kornreich, A. Hernandez-Garcia, I. K. Voets, R. Beck, M. A. C. Stuart, F. A. M. Leermakers and R. de Vries, *J. Phys. Chem. B*, 2015, **119**, 4084–4092.

44 T. Stephan, S. Muth and M. Schmidt, *Macromolecules*, 2002, **35**, 9857–9860.

45 I. Erukhimovich, P. E. Theodorakis, W. Paul and K. Binder, *J. Chem. Phys.*, 2011, **134**, 054906.

46 O. V. Borisov, E. B. Zhulina and T. M. Birshtein, *ACS Macro Lett.*, 2012, **1**, 1166–1169.

47 S. C. Radzinski, J. C. Foster, S. J. Scannelli, J. R. Weaver, K. J. Arrington and J. B. Matson, *ACS Macro Lett.*, 2017, **6**, 1175–1179.

48 D. J. Walsh and D. Guironnet, *Proc. Natl. Acad. Sci. U.S.A.*, 2019, 201817745.

49 E. B. Zhulina and T. A. Vilgis, *Macromolecules*, 1995, **28**, 1008–1015.

50 Y. Rouault and O. V. Borisov, *Macromolecules*, 1996, **29**, 2605–2611.

51 M. Saariaho, O. Ikkala, I. Szleifer, I. Erukhimovich and G. ten Brinke, *J. Chem. Phys.*, 1997, **107**, 3267–3276.

52 M. Saariaho, A. Subbotin, I. Szleifer, O. Ikkala and G. ten Brinke, *Macromolecules*, 1999, **32**, 4439–4443.

53 P. G. Khalatur, D. G. Shirvanyanz, N. Y. Starovoitova and A. R. Khokhlov, *Macromol. Theory Simul.*, 2000, **9**, 141–155.

54 A. Yethiraj, *J. Chem. Phys.*, 2006, **125**, 204901.

55 J. Paturej and T. Kreer, *Soft Matter*, 2017, **13**, 8534–8541.

56 M. Saariaho, O. Ikkala and G. ten Brinke, *J. Chem. Phys.*, 1999, **110**, 1180–1187.

57 K. Shiokawa, K. Itoh and N. Nemoto, *J. Chem. Phys.*, 1999, **111**, 8165–8173.

58 S. Elli, F. Ganazzoli, E. G. Timoshenko, Y. A. Kuznetsov and R. Connolly, *J. Chem. Phys.*, 2004, **120**, 6257–6267.

59 D. Chatterjee and T. A. Vilgis, *Macromol. Theory Simul.*, 2016, **25**, 518–523.

60 Y. Nakamura and T. Norisuye, *Polym. J.*, 2001, **33**, 874–878.

61 L. Feuz, F. A. M. Leermakers, M. Textor and O. Borisov, *Macromolecules*, 2005, **38**, 8891–8901.

62 N. A. Denesyuk, *Phys. Rev. E*, 2003, **68**, 1293–11.

63 N. A. Denesyuk, *Phys. Rev. E*, 2003, **67**, 5201–10.

64 W. F. M. Daniel, J. Burdyńska, M. Vatankhah-Varnoosfaderani, K. Matyjaszewski, J. Paturej, M. Rubinstein, A. V. Dobrynin and S. S. Sheiko, *Nat. Mater.*, 2015, **15**, 183–189.

65 S. J. Dalsin, T. G. Rions-Maehren, M. D. Beam, F. S. Bates, M. A. Hillmyer and M. W. Matsen, *ACS Nano*, 2015, **9**, 12233–12245.

66 Z. Cao, J.-M. Y. Carrillo, S. S. Sheiko and A. V. Dobrynin, *Macromolecules*, 2015, **48**, 5006–5015.

67 J. Paturej, S. S. Sheiko, S. Panyukov and M. Rubinstein, *Sci. Adv.*, 2016, **2**, e1601478–e1601478.

68 M. Abbasi, L. Faust, K. Riazi and M. Wilhelm, *Macromolecules*, 2017, **50**, 5964–5977.

69 H. Liang, Z. Cao, Z. Wang, S. S. Sheiko and A. V. Dobrynin, *Macromolecules*, 2017, **50**, 3430–3437.

70 T.-P. Lin, A. B. Chang, S.-X. Luo, H.-Y. Chen, B. Lee and R. H. Grubbs, *ACS Nano*, 2017, **11**, 11632–11641.

71 I. N. Haugan, M. J. Maher, A. B. Chang, T.-P. Lin, R. H. Grubbs, M. A. Hillmyer and F. S. Bates, *ACS Macro Lett.*, 2018, **7**, 525–530.

72 B. Zhang, F. Gröhn, J. S. Pedersen, K. Fischer and M. Schmidt, *Macromolecules*, 2006, **39**, 8440–8450.

73 L. Feuz, P. Strunz, T. Geue, M. Textor and O. Borisov, *Eur. Phys. J. E*, 2007, **23**, 237–245.

74 S. L. Pesek, Q. Xiang, B. Hammouda and R. Verduzco, *J. Polym. Sci., Part B: Polym. Phys.*, 2017, **55**, 104–111.

75 S. Lecommandoux, F. Chécot, R. Borsali, M. Schappacher, A. Deffieux, A. Brûlet and J. P. Cotton, *Macromolecules*, 2002, **35**, 8878–8881.

76 A. P. Filippov, A. S. Krasova, E. B. Tarabukina, A. V. Kashina, T. K. Meleshko and A. V. Yakimansky, *J. Polym. Res.*, 2016, **23**, 1–9.

77 F. Dutertre, K.-T. Bang, B. Loppinet, I. Choi, T.-L. Choi and G. Fytas, *Macromolecules*, 2016, **49**, 2731–2740.

78 L. Grebikova, S. Kozhuharov, P. Maroni, A. Mikhaylov, G. Dietler, A. D. Schlüter, M. Ullner and M. Borkovec, *Nanoscale*, 2016, **8**, 13498–13506.

79 H.-P. Hsu, W. Paul and K. Binder, *Macromol. Theory Simul.*, 2007, **16**, 660–689.

80 H.-P. Hsu, W. Paul and K. Binder, *Macromolecules*, 2010, **43**, 3094–3102.

81 H.-P. Hsu, W. Paul, S. Rathgeber and K. Binder, *Macromolecules*, 2010, **43**, 1592–1601.

82 P. E. Theodorakis, H.-P. Hsu, W. Paul and K. Binder, *J. Chem. Phys.*, 2011, **135**, 164903–14.

83 K. Binder, H.-P. Hsu and W. Paul, *Eur. Phys. J.: Spl. Top.*, 2016, **225**, 1663–1671.

84 Y. Nakamura and T. Norisuye, *Soft Matter Characterization*, Springer Netherlands, Dordrecht, 2008, pp. 235–286.

85 H.-P. Hsu, W. Paul and K. Binder, *J. Chem. Phys.*, 2008, **129**, 204904.

86 K. Binder, H.-J. Butt, G. Floudas, H. Frey, H.-P. Hsu, K. Landfester, U. Kolb, A. Kühnle, M. Maskos, K. Müllen, W. Paul, M. Schmidt, H. W. Spiess and P. Virnau, *From Single Molecules to Nanoscopically Structured Materials*, Springer International Publishing, 2013, pp. 115–210.

87 J. A. Love, J. P. Morgan, T. M. Trnka and R. H. Grubbs, *Angew. Chem. Int. Ed.*, 2002, **41**, 4035–4037.

88 J. M. Blanco, F. Fernández, X. García-Mera and J. E. Rodríguez-Borges, *Tetrahedron*, 2002, **58**, 8843–8849.

89 T.-L. Choi and R. H. Grubbs, *Angew. Chem. Int. Ed.*, 2003, **42**, 1743–1746.

90 E. O. Kraemer, *Ind. Eng. Chem.*, 1938, **30**, 1200–1203.

91 M. L. Huggins, *J. Am. Chem. Soc.*, 1942, **64**, 2716–2718.

92 L. M. Polgar, H. Lentzakis, D. Collias, F. Snijkers, S. Lee, T. Chang, G. Sakellariou, D. A. Z. Wever, C. Toncelli, A. A. Broekhuis, F. Picchioni, A. D. Gotsis and D. Vlassopoulos, *Macromolecules*, 2015, **48**, 6662–6671.

93 K. Nishi, S. Tochioka, T. Hiroi, T. Yamada, K. Kokado, T.-H. Kim, E. P. Gilbert, K. Sada and M. Shibayama, *Macromolecules*, 2015, **48**, 3613–3621.

94 H. Unsal, S. Onbulak, F. Calik, M. Er-Rafik, M. Schmutz, A. Sanyal and J. Rzayev, *Macromolecules*, 2017, **50**, 1342–1352.

95 K. Kremer and G. S. Grest, *J. Chem. Phys.*, 1990, **92**, 5057–5086.

96 J. D. Weeks, D. Chandler and H. C. Andersen, *J. Chem. Phys.*, 1971, **54**, 5237–5247.

97 R. Auhl, R. Everaers, G. S. Grest, K. Kremer and S. J. Plimpton, *J. Chem. Phys.*, 2003, **119**, 12718–12728.

98 D. L. Ermak and J. A. McCammon, *J. Chem. Phys.*, 1978, **69**, 1352–1360.

99 B. Dünweg, D. Reith, M. Steinhauser and K. Kremer, *J. Chem. Phys.*, 2002, **117**, 914–924.

100 R. R. Schmidt, J. G. H. Cifre and J. G. de la Torre, *Eur. Phys. J. E*, 2012, **35**, 130.

101 J. G. de la Torre, M. C. L. Martinez and M. M. Tirado, *Macromolecules*, 1984, **17**, 2715–2722.

102 K. Tsuda, *Rheol. Acta*, 1970, **9**, 509–516.

103 B. Carrasco and J. G. de la Torre, *Biophys. J.*, 1999, **76**, 3044–3057.

104 B. Liu and B. Dünweg, *J. Chem. Phys.*, 2003, **118**, 8061–8072.

105 M. Rubinstein and R. Colby, *Polymer physics*, Oxford University Press, N. Y., 2003.

106 J. R. Dorgan, J. Janzen, D. M. Knauss, S. B. Hait, B. R. Limoges and M. H. Hutchinson, *J. Polym. Sci., Part B: Polym. Phys.*, 2005, **43**, 3100–3111.

107 T. F. A. Haselwander, W. Heitz, S. A. Krügel and J. H. Wendorff, *Macromol. Chem. Phys.*, 1996, **197**, 3435–3453.

108 C. Svaneborg, H. A. Karimi-Varzaneh, N. Hojdis, F. Fleck and R. Everaers, *Phys. Rev. E*, 2016, **94**, 032502.

109 B. G. G. Lohmeijer, R. C. Pratt, F. Leibfarth, J. W. Logan, D. A. Long, A. P. Dove, F. Nederberg, J. Choi, C. Wade, R. M. Waymouth and J. L. Hedrick, *Macromolecules*, 2006, **39**, 8574–8583.

110 C. W. Bielawski and R. H. Grubbs, *Prog. Polym. Sci.*, 2007, **32**, 1–29.

111 M. Wintermantel, M. Schmidt, Y. Tsukahara, K. Kajiwara and S. Kohjiya, *Macromol. Rapid Commun.*, 1994, **15**, 279–284.

112 K. Terao, T. Hokajo, Y. Nakamura and T. Norisuye, *Macromolecules*, 1999, **32**, 3690–3694.

113 A. Stukowski, *Modell. Simul. Mater. Sci. Eng.*, 2009, **18**, 015012.

114 T. Lesné, V. Heroguez, Y. Gnanou and R. Duplessix, *Colloid Polym. Sci.*, 2001, **279**, 190–195.

115 M. Hu, Y. Xia, G. B. McKenna, J. A. Kornfield and R. H. Grubbs, *Macromolecules*, 2011, **44**, 6935–6943.

116 S. J. Dalsin, M. A. Hillmyer and F. S. Bates, *ACS Macro Lett.*, 2014, **3**, 423–427.

117 J. W. Cannon, J. A. Aronovitz and P. Goldbart, *J. Phys. I*, 1991, **1**, 629–645.

118 O. Jagodzinski, E. Eisenriegler and K. Kremer, *J. Phys. I*, 1992, **2**, 2243–2279.

119 P. E. Theodorakis and N. G. Fytas, *Am. J. Condens. Matter Phys.*, 2012, **2**, 101–108.

120 V. Blavatska, C. von Ferber and Y. Holovatch, *Condens. Matter Phys.*, 2011, **14**, 33701.

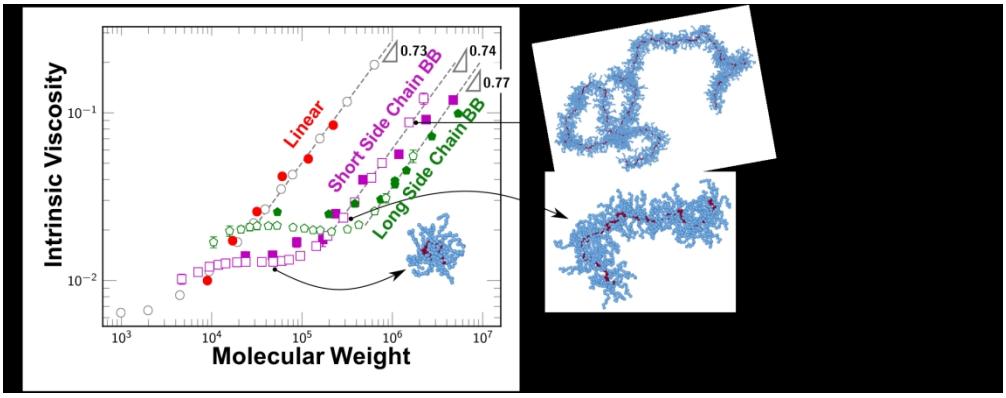
Intrinsic Viscosity
Molecular Weight
Linear
Short Side Chain BB
Long Side Chain BB
0.73
0.74
0.77